Biophysical Journal
Article

Biophysical Society

Investigation of LRRC8-Mediated Volume-Regulated Anion Currents in *Xenopus* Oocytes

Héctor Gaitán-Peñas,[1,2] Antonella Gradogna,[3] Lara Laparra-Cuervo,[4] Carles Solsona,[5] Victor Fernández-Dueñas,[6] Alejandro Barrallo-Gimeno,[1,2] Francisco Ciruela,[6] Melike Lakadamyali,[4] Michael Pusch,[3,*] and Raúl Estévez[1,2,*]

[1]Unitat de Fisiología, Departament de Ciències Fisiològiques II, IDIBELL-Universitat de Barcelona, L'Hospitalet de Llobregat, Spain; [2]U-750, CIBERER, ISCIII, Spain; [3]Istituto di Biofisica, CNR, Genoa, Italy; [4]ICFO-Institut de Ciències Fotòniques, The Barcelona Institute of Science and Technology, Castelldefels, Spain; [5]Unitat de Neurobiologia and [6]Unitat de Farmacologia, Departament Patologia i Terapèutica Experimental IDIBELL-Universitat de Barcelona, L'Hospitalet de Llobregat

ABSTRACT Volume-regulated anion channels (VRACs) play an important role in controlling cell volume by opening upon cell swelling. Recent work has shown that heteromers of LRRC8A with other LRRC8 members (B, C, D, and E) form the VRAC. Here, we used *Xenopus* oocytes as a simple system to study LRRC8 proteins. We discovered that adding fluorescent proteins to the C-terminus resulted in constitutive anion channel activity. Using these constructs, we reproduced previous findings indicating that LRRC8 heteromers mediate anion and osmolyte flux with subunit-dependent kinetics and selectivity. Additionally, we found that LRRC8 heteromers mediate glutamate and ATP flux and that the inhibitor carbenoxolone acts from the extracellular side, binding to probably more than one site. Our results also suggest that the stoichiometry of LRRC8 heteromers is variable, with a number of subunits ≥ 6, and that the heteromer composition depends on the relative expression of different subunits. The system described here enables easy structure-function analysis of LRRC8 proteins.

INTRODUCTION

As a consequence of volume changes, cells activate regulatory mechanisms involving several transporters and ion channels to restore their original size (1). These mechanisms are named regulatory volume increase and regulatory volume decrease (RVD) (2). The process of RVD relies on a swelling-induced increase in the activity of a volume-regulated anion channel (VRAC) that releases organic osmolytes and anions, accompanied by the release of K^+ ions through potassium channels, and followed by osmotically driven water efflux. The anion channel has also been called the volume-sensitive organic osmolyte-anion channel (VSOAC) or the volume-sensitive outwardly rectifying anion channel (VSOR) (3). We will refer to it in the following as the VRAC.

The biophysical properties of VRACs have been extensively studied (3–6). VRAC-mediated currents activate slowly under extracellular hypotonic challenge showing a moderate instantaneous outward rectification, which reflects voltage dependence of the single-channel conductance and inactivation at positive voltages (7). Nonspecific inhibitors, such as DCPIB (8,9) or carbenoxolone (CBX) (10), which is also a gap junction blocker (11,12) and pannexin blocker (13), are found to block VRACs.

The molecular identification of the proteins responsible for VRAC activity has been finally achieved after a long history of false positives (14,15). Two groups independently identified heteromers of the leucine-rich-repeat-containing 8, member A (LRRC8A) protein with other members of the LRRC8 family (B, C, D, and E) as components of VRACs (16,17). LRRC8B–E require coexpression with LRRC8A for plasma membrane delivery (17). The subunit composition of LRRC8 heteromers affects some channel properties, such as depolarization-dependent inactivation (18), substrate specificity (17,19), and single-channel conductance (20).

Investigating the functional properties of VRAC activity induced by LRRC8 proteins is challenging. VRAC currents have been found in most vertebrate cell lines examined (14). To study LRRC8A, it was necessary to complement siRNA-depleted (16) or genome-edited cell lines (17), as the

Submitted May 11, 2016, and accepted for publication August 26, 2016.

*Correspondence: pusch@ge.ibf.cnr.it or restevez@ub.edu

Héctor Gaitán-Peñas and Antonella Gradogna contributed equally to this work.

Michael Pusch and Raúl Estévez contributed equally to this work.

Editor: William Kobertz.

http://dx.doi.org/10.1016/j.bpj.2016.08.030

overexpression of LRRC8A suppressed the endogenous VRAC activity in cell lines by an unknown mechanism (16,17). Furthermore, the study of LRRC8 heteromers required knocking out all five LRRC8 genes by genome editing (17,20). More recently, LRRC8 heteromers have also been studied after functional reconstitution in droplet lipid bilayers (20). In addition, LRRC8 currents activate slowly by hypotonicity (17), resulting in nonsteady current levels, which complicates quantitative analysis.

In this work, we describe an alternative approach to functionally characterize VRAC activity induced by LRRC8 proteins in *Xenopus* oocytes. With this approach, we were able to perform a detailed biophysical characterization including subunit dependence of current kinetics and ion selectivity, single-channel conductance, osmolyte influx, ATP efflux, inhibitor sensitivity, osmolarity dependence, and stoichiometry.

MATERIALS AND METHODS

Molecular biology

Plasmids presented herein were constructed using standard molecular biology techniques employing recombinant polymerase chain reaction and the Multisite Gateway system (Invitrogen, Carlsbad, CA). The integrity of all constructs was confirmed by DNA sequencing.

For expression in *Xenopus* oocytes, after linearization by NotI, complementary RNA (cRNA) of human LRRC8 proteins was transcribed using the mMessage mMachine SP6 kit (Ambion, Waltham, MA). We produced cRNA of LRRC8A/B/C/D/E constructs and hLRRC8A/E-VFP and hLRRC8A/B/C/D/E-monomeric Cherry (mCherry) fluorescent constructs. They were expressed by themselves or coexpressed mainly with LRRC8A or LRRC8A-VFP.

Oocyte preparation and injection

Oocytes were harvested from *Xenopus laevis* frogs that had been anesthetized by tricaine (ethyl 3-aminobenzoate methanesulfonate salt; Sigma Aldrich, St. Louis, MO) at a concentration of 1.5 gL^{-1} buffered to neutral pH with sodium bicarbonate. After surgery, frogs were allowed to recover from anesthesia, and suitable aftercare was given. All animal protocols conformed to the European Community Guidelines on Animal Care and Experimentation and were approved by the Ethics Committee for Animal Experimentation of the University of Barcelona for the experiments conducted in Barcelona and by the Ethics Committee for Animal Experimentation of the Biophysics Institute for the experiments conducted in Genoa. Oocytes were enzymatically defolliculated by an ~1 h treatment with collagenase type I A from *Clostridium histolyticum* (Sigma Aldrich) in a solution containing (in mM) 90 NaCl, 2 KCl, 1 $MgCl_2$, and 10 Hepes at pH 7.5 with gentle shaking at room temperature. Fifty nanoliters of cRNA, normally containing 12 ng of each subunit, was injected with a microinjector (Nanoject II, Drummond Scientific, Broomall, PA).

Electrophysiology (voltage clamp)

After cRNA injection, oocytes were maintained at 18°C in a solution containing (in mM) 90 NaCl, 2 KCl, 1 $MgCl_2$, 1 $CaCl_2$, and 10 Hepes at pH 7.5 or in modified Barth's solution that contained (in mM) 88 NaCl, 1 KCl, 0.41 $CaCl_2$, 0.82 $MgSO_4$, 0.33 $Ca(NO_3)_2$, 2.4 $NaHCO_3$, and 10 Hepes at pH 7.4 containing 10 mg/mL of gentamicin. One to three days after injection, voltage-clamp measurements were performed by using the custom acquisition program GePulse (available at http://users.ge.ibf.cnr.it/pusch/programs-mik.htm) or the program CellWorks (Npi Electronic, Tamm, Germany) and a Turbo TEC-03X or Tec-05X amplifier (Npi Electronic). To estimate the expression level of the constructs varying the osmolarity, different solutions were prepared containing (in mM) 48 NaCl, 2 KCl, 1.8 $CaCl_2$, 1 $MgCl_2$, and 10 Hepes at pH 7.3 (osmolarity, 120 mOsm), called "Hypo"; "Hypo" was supplemented with mannitol to obtain the "Iso" solution (osmolarity, 200 mOsm) and the "Hyper" solution (osmolarity, 310 mOsm). The investigation of the osmolarity dependence of 8A-VFP/8E-mCherry required additional solutions containing (in mM) 24 NaCl, 2 KCl, 1.8 $CaCl_2$, 1 $MgCl_2$, and 10 Hepes at pH 7.3 (osmolarity, 74 mOsm), and 7 NaCl, 2 KCl, 1.8 $CaCl_2$, 1 $MgCl_2$, and 10 Hepes at pH 7.3 (osmolarity, 40 mOsm).

The standard bath solution used for the selectivity measurements contained (in mM) 100 NaCl, 5 $MgSO_4$, and 10 Hepes at pH 7.3 (osmolarity, 215 mOsm). The selectivity to the different ions was estimated substituting sodium chloride with sodium iodide, nitrate, bromide, glutamate, gluconate, bicarbonate, thiocyanate, fluoride, and lactate. Similarly, sodium selectivity was tested by substituting sodium chloride with tetraethylammonium chloride (TEA-Cl). For taurine and glycine, which are neutral at pH 7, we prepared solutions at alkaline pH containing (in mM) 140 taurine, 64 NMDG (N-methyl-D-glucamine), and 5 $MgSO_4$ at pH 9, and 159 glycine, 38 NMDG, and 5 $MgSO_4$ at pH 9.3, respectively. Based on previous work (4), the concentration of the negatively charged species was calculated as 78 mM for the taurine solution and 53 mM for the glycine solution assuming pKa values of 8.9 for taurine and 9.6 for glycine, respectively. The selectivity of the LRRC8 constructs was estimated based on the reversal potential change resulting from the replacement of the standard bath solution with the desired solution. Liquid junction potentials were measured and subtracted.

For the selectivity measurements. the reversal potential was determined applying voltages ranging from −60 to 50 mV with 10 mV increments for 50 ms and fitting a parabola to the four points nearest to the zero current potential. The selectivity was estimated according to the Goldman-Hodgkin-Katz equation (21), which for Cl^- replacement with different ions became

$$\frac{Px}{P_{Cl}} = \frac{[Cl]}{[x]} \times e^{-\frac{\Delta E_r F}{RT}}, \quad (1)$$

where P_x and P_{Cl} are the permeability of the ion tested and of Cl^-, [Cl] and [x] are concentrations of Cl^- and the x ion, and ΔE_r is the shift of the estimated reversal potential. When we replaced NaCl with TEA-Cl, the formula became

$$\frac{P_{Na}}{P_{Cl}} = \frac{[Cl]_{int}}{[Na_0]_{out}} \times \left(e^{-\frac{\Delta E_r F}{RT}} - 1\right), \quad (2)$$

where P_{Na} and P_{Cl} are the permeability of Na^+ and Cl^-, $[Cl]_{int}$ and $[Na_0]_{out}$ are the Cl^- concentration inside the oocyte (~30 mM) and the initial external Na^+ concentration (100 mM), respectively. Here, we assumed that TEA is completely impermeable (compared to sodium).

To estimate LRRC8-mediated currents at different potentials, the "IV-pulse protocol" was applied: a prepulse to −100 mV for 200 ms was followed by voltages ranging from −100 to 60 mV with 20 mV increments for 3000 ms. Pulses ended with a tail to −70 mV for 500 ms.

To study the effect of CBX, we applied increasing concentrations of CBX (10, 20, 50, 100, and 500 μM) dissolved in the "Iso" solution, performing the solution changes when the current was almost at steady state (see Fig. 6 *A*). To quantify the blocking effect of CBX, the steady-state current at various CBX concentrations was estimated by extrapolating to

infinite time an exponential function fitted to the time course of the onset of block (see Fig. 6 *A*). The steady-state current was normalized to the initial current in the "Iso" solution (see Fig. 6 *B*) and fitted to the Hill equation of the form

$$p_u = \frac{1 - p_\infty}{1 + \left(\frac{[CBX]}{K_A}\right)^n} + p_\infty, \quad (3)$$

where p_u is the probability of not being blocked by CBX, [CBX] is the CBX concentration, K_A the apparent binding constant, n is the Hill coefficient, and p_∞ takes into account the leak currents remaining after complete blockage.

Electrophysiology (patch clamp)

For patch clamp, the vitelline membrane was mechanically removed by small forceps. To achieve this, oocytes were bathed in a slightly hypertonic medium obtained by mixing a standard shrinking solution (containing (in mM) 200 Na-Aspartate, 20 KCl, 1 $MgCl_2$, 5 EGTA, and 10 Hepes, pH 7.3) with the patch-clamp bath solution (see below) in a 1:2 ratio, resulting in an osmolarity of ~280 mOsm. Oocytes were kept in this solution for at most 2 min.

Single-channel measurements were performed by patch clamp in the cell-attached configuration. The bath solution contained (in mM) 100 N-methyl-D-glucamine-Cl (NMDG-Cl), 2 $MgCl_2$, 1 EGTA, and 10 Hepes at pH 7.3. The extracellular solution (in the pipette) was the same "Iso" solution used for voltage-clamp measurements, containing (in mM) 48 NaCl, 2 KCl, 1.8 $CaCl_2$, 1 $MgCl_2$, and 10 Hepes at pH 7.3 supplemented with mannitol to obtain an osmolarity of 200 mOsm. Pipettes were pulled from aluminosilicate glass capillaries (Hilgenberg, Malsfeld, Germany) and had resistances of 3–5 MOhm in the recording solution. To record single-channel events at different potentials, repetitive pulses ranging from 80 to -80 mV with -20 mV increments for 1000 msec were applied 10-30 times. Currents were recorded at 50 kHz after filtering at 3 kHz with an eight-pole Bessel filter. The single-channel analysis was performed by concatenating the traces recorded at the same potential and estimating the current levels by manually fitting a superposition of Gaussian distributions.

To quantify the inhibitory effect of CBX, patch-clamp measurements were performed in the outside-out configuration. The intracellular solution (in the pipette) contained (in mM) 100 N-methyl-D-glucamine-Cl (NMDG-Cl), 2 $MgCl_2$, 1 EGTA, and 10 Hepes at pH 7.3. The extracellular solution was the "Iso" solution. CBX was dissolved in the "Iso" solution at 100 μM. Pipettes were pulled from aluminosilicate glass capillaries (Hilgenberg) and had resistances of 7–9 MOhm in the recording solution. The perfusion was performed by using glass capillaries mounted on a rod that can be quickly moved allowing fast changes of the solution directly on the patch. To evaluate the effect of CBX, currents were evoked with repetitive 400 ms pulses to 80 mV delivered once per 1.3 s. Currents recorded in CBX were normalized to the steady-state currents measured at 80 mV in control conditions. Error bars indicate the standard deviation.

Western blot

Thirty oocytes were homogenized by 20 strokes in an Eppendorf Teflon-glass homogenizer in 10 μL/oocyte of buffer containing 1% TX-100, 150 mM NaCl, and phosphate-buffered saline plus protease inhibitors. The homogenate was centrifuged twice at 1000 $\times$ *g* for 10 min at 4°C to eliminate the yolk. The proteins in the supernatant were quantified by the BCA method. Sodium dodecyl sulfate polyacrylamide gel electrophoresis and Western blot experiments were performed as described (22), loading 100 μg of extract. We used the antibodies anti-GFP (ab290, AbCAM, Cambridge, United Kingdom), anti-Cherry (ab125096, AbCAM), and anti-tubulin (MMS-435P, Covance Antibody Products, Princeton, NJ) at 1:100 dilution.

Uptake measurements

To measure uptake of [2,2-^{3}H]-taurine, L-[3,4-^{3}H]-glutamate, and [2-^{3}H]-glycine (NEN Radiochemicals, PerkinElmer, Waltham, MA), seven oocytes per individual data point were first incubated for 10 min in Na1X isosmotic solution containing (in mM) 100 NaCl, 2 KCl, 1 $CaCl_2$, 1 $MgCl_2$, and 10 Hepes/Tris, pH 7.5, or in Na0.5X hypotonic solution (obtained by diluting the Na1X solution 1:1 with water). To initiate uptake, oocytes were transferred into 90 μL Na1X or 90 μL Na0.5X solution supplemented with 100 μM of substrate at 1 μCi/mL, and incubated at 25°C for 20 min. After incubation, the uptake solution was removed, and the oocytes were washed three times in 4 mL ice-cold Na1X solution supplemented with 1 mM substrate. Immediately, each single oocyte was inserted into a scintillation vial and dissolved in 200 μL of 10% sodium dodecyl sulfate, and the radioactivity was counted after the addition of 3 ml of scintillation fluid.

Water permeability measurements

Water permeability was assessed by placing individual oocytes into small plates containing hypotonic ND48 medium (ND96/2). This was a two-step procedure in which we first equilibrated the internal osmolarity to isosmotic ND48 with mannitol (190 mOsm), and later placed the oocyte into ND48 (95 mOsm). Oocyte swelling was recorded by a Nikon CDSS230 stereomicroscope coupled to a Nikon DS-U2 camera. NIS Elements software was used to configure the imaging protocol for data acquisition. Oocyte volume was obtained from the oocyte section area calculated in ImageJ. Water permeability (Pf) was calculated from the initial rate of volume increase with the formula $Pf = V_o[d(V/V_o)/dt]/[S_o \times V_m (Osm_{in} - Osm_{out})]$, where V_o is the initial oocyte volume (in cm^3), S_o the initial oocyte area (in cm^2), V_m the molar volume of water (18 cm^3/mol), Osm_{in} the internal oocyte osmolarity (190 mOsm), and Osm_{out} the ND48 osmolarity.

ATP release

ATP release from hypotonically challenged oocytes was measured using a Luciferase and D-Luciferin mixture (LL). Luciferase extract lantern from *Photinus pyralis* (Sigma Aldrich) was resuspended at a concentration of 0.1 μg/μL and desalted in a 10 mL 10 DG column (Biorad, Hercules, CA). D-Luciferin (Sigma Aldrich) was diluted at a concentration of 0.7 μg/μL in ultrapure water and the pH was adjusted to 7.4 with NaOH.

In a homemade recording chamber, a hemolysis tube was placed that contained 500 μL of the test solution and 5 μL of D-luciferin and 5 μL of luciferase. Usually, two oocytes were immersed in the tube. Light emitted when ATP reacted with LL was captured by a photomultiplier (R374, Hamamatsu, Hamamatsu City, Japan) fed at high voltage (700–800 V). The resulting signal was amplified in a low-noise amplifier (P16, Grass Valley, Las Cruces, NM), filtered at 10 Hz with a Bessel filter (Frequency Devices, Ottawa, IL), and digitized at 50 Hz using WinWCP (v3.3.3) software (from Professor John Dempster, Strathclyde University, Glasgow, United Kingdom). The amount of ATP released after 7 min was calculated taking into account the signal of standard amounts of ATP in the same experimental conditions. The recording chamber is illustrated in detail in Fig. S1 in the Supporting Material.

Single-step photobleaching methods

Images of the oocytes were acquired on a custom-built total internal reflection fluorescence (TIRF) microscope based on an Olympus (Center Valley, PA) IX71 inverted microscope frame fitted with a 100×, 1.4 NA

oil-immersion objective. Excitation light at 488 nm from an Argon-Krypton laser (Coherent, Santa Clara, CA) was used to excite the Venus fluorescent protein (VFP) in TIRF mode. Excitation light at 560 nm from a fiber laser (MPB Communications, Montreal, Canada) was used to excite mCherry in TIRF mode. Emission of VFP was collected with a BP 525/50 emission filter (Chroma Technology, Bellows Falls, VT) and that of mCherry was collected with BP 605/52 (Chroma Technology). The fluorescence emission was recorded onto an EMCCD camera (pixel size, 157 nm) (Andor Technology, Belfast, United, Kingdom) with an exposure time of 100 ms/frame.

The single-step photobleaching images were achieved by exposing first mCherry to 560 nm laser light at 7.9 W/cm^2 until all were photobleached, and then, in the same field of view, VFP to 488 nm laser light at 3.2 W/cm^2 until all were photobleached.

For the analysis of the step-photobleaching data, a square region of 3 × 3 pixels around the center of each spot was chosen to extract intensity-time traces using custom-written Python software. Background was subtracted locally by considering the average intensity of a 2 × 2 pixel region surrounding the molecule of interest. We excluded from our analysis spots that moved by >1 pixel before they photobleached, spots that were fluorescent for only one frame, and multiple partially overlapping spots. The signal/noise ratio was ~3, and it has been shown previously that the counting in step bleaching methods is reliable as long as the signal/noise ratio is 1.5 or above (23). The steps in intensity-time traces were counted manually, as previous work (24) has indicated that automated fitting (25) is not as reliable for this type of data. Photobleaching steps were defined as events in which the mean intensity of the smallest step was greater than at least two standard deviations from the background fluorescence. The intensity of an individual step was determined from traces containing only a single step and was 6.2 ± 1.6 a.u. for VFP. This intensity was used as a cut-off to define single steps. Steps that had an intensity greater than two standard deviations away from this mean intensity were likely due to missed events in which multiple fluorescent proteins photobleached simultaneously and these traces were not considered in the analysis. The resulting distribution of the number of steps was compared to either a binomial distribution (Eq. 4) or a Poisson distribution (Eq. 5):

$$q_n = \left(\frac{M!}{n!(M-n)!}\right)P^n(1-P)^{M-n} \tag{4}$$

$$q_n = \frac{\lambda^n e^{-\lambda}}{n!} \tag{5}$$

In Eqs. 4 and 5, q_n is the probability of observing n steps in a time trace. In Eq. 4, M is the total number of subunits and P is the probability that the fluorescent protein will be fluorescent. In Eq. 5, λ is the average number of subunits (26). The distribution should follow binomial statistics if the stoichiometry of the subunits is fixed and a Poisson distribution if the stoichiometry is free (23,26). A possible caveat of the photobleaching method is that incomplete folding efficiency of the fluorescent protein can cause a systematic underestimation of the number of subunits (27). We previously showed that VFP folds and matures with high efficiency (~80%) in *Xenopus* oocytes under similar cytosolic tagging and imaging conditions using the human glycine receptor (23,24), and we could reliably determine the pentameric stoichiometry of homomeric α-subunit expressed alone, as well as the 3:2 stoichiometry of heteromeric α/β complexes (23). VFP folding efficiency was independent of the type and oligomeric state of the tagged subunit (23,24). Given these results, we relied on the photobleaching of VFP to assess the LRRC8 subunit stoichiometry.

To determine the density of LRRC8 subunits per unit area, the total number of fluorescent spots in 40 μm × 40 μm fields of view (FOVs) was counted manually for mCherry as well as for VFP. A spot was considered if its intensity was within the intensity range of a single photobleaching step. In addition, the number of mCherry and VFP spots that colocalized was counted from those spots that shared the same 3 × 3 pixel region in the two channels. Once again, we excluded spots that were fluorescent for only one frame and multiple partially overlapping ones in the same region of interest.

RESULTS

First studies of expression of LRRC8 proteins in *Xenopus* oocytes

The recent identification of the members of the LRRC8 family as the molecular correlates of VRAC (16,17) allows the molecular characterization of the proteins underlying these channels. In this work, we took advantage of the fact that enzymatically defolliculated *Xenopus* oocytes have no endogenous VRAC-like current (8,28,29) to perform a characterization of LRRC8 proteins expressed in these cells. For simplification, we named LRRC8A as 8A and the other isoforms analogously.

We first verified that collagenase-defolliculated uninjected oocytes do not express endogenous VRAC: both in isotonic conditions (200 mOsm) and under continued perfusion with hypotonic solution (120 mOsm) for 10 min, no significant currents were activated (Fig. 1 *A*). Injection of 8A or 8E RNA alone did not induce VRAC currents (Fig. 1, *B* and *C*). Also, currents in 8A and 8E coinjected oocytes were practically indistinguishable from endogenous currents in isotonic conditions (Fig. 1 *D*, *left*). However, in contrast to oocytes expressing 8A or 8E alone (Fig. 1, *B* and *C*), currents in 8A and 8E coinjected oocytes slowly activated in hypotonic conditions (Fig. 1 *D*; Fig. S2 *A*). Hypotonicity-induced 8A/8E currents showed outward rectification of the initial current upon the voltage step (instantaneous rectification) and slow inactivation at positive potentials, in agreement with properties found in several mammalian cell lines (5). After the activation by hypotonicity, 8A/8E-mediated currents returned slowly to the initial current level upon application of the isotonic solution (Fig. S2 *A*).

We next coexpressed 8A with the other related homologs, 8B, 8C, and 8D. 8A/8B (Fig. S3 *A*) and 8A/8C (Fig. S3 *B*) did not show significant currents either in isotonic conditions or under prolonged exposure to hypotonic solution. Similarly, 8A/8D-induced currents were very small and comparable to those of uninjected oocytes in isotonic conditions. Nevertheless, upon hypotonic stimulation, significant currents could be evoked (Fig. S3 *C*). However the functional expression level of 8A/8D (Fig. S3 *C*) was lower compared to 8A/8E (Fig. 1 *D*).

For the purpose of studying stoichiometry and localization of these heteromers, LRRC8 proteins C-terminally tagged with VFP or with mCherry (*mCh* in the figures) were prepared. Surprisingly, the addition of fluorescent proteins to the C-terminus dramatically increased 8A/8E activity. Indeed, the heteromer 8A-VFP/8E-mCherry exhibited consistent currents even in isotonic conditions (Fig. 1 *E*)

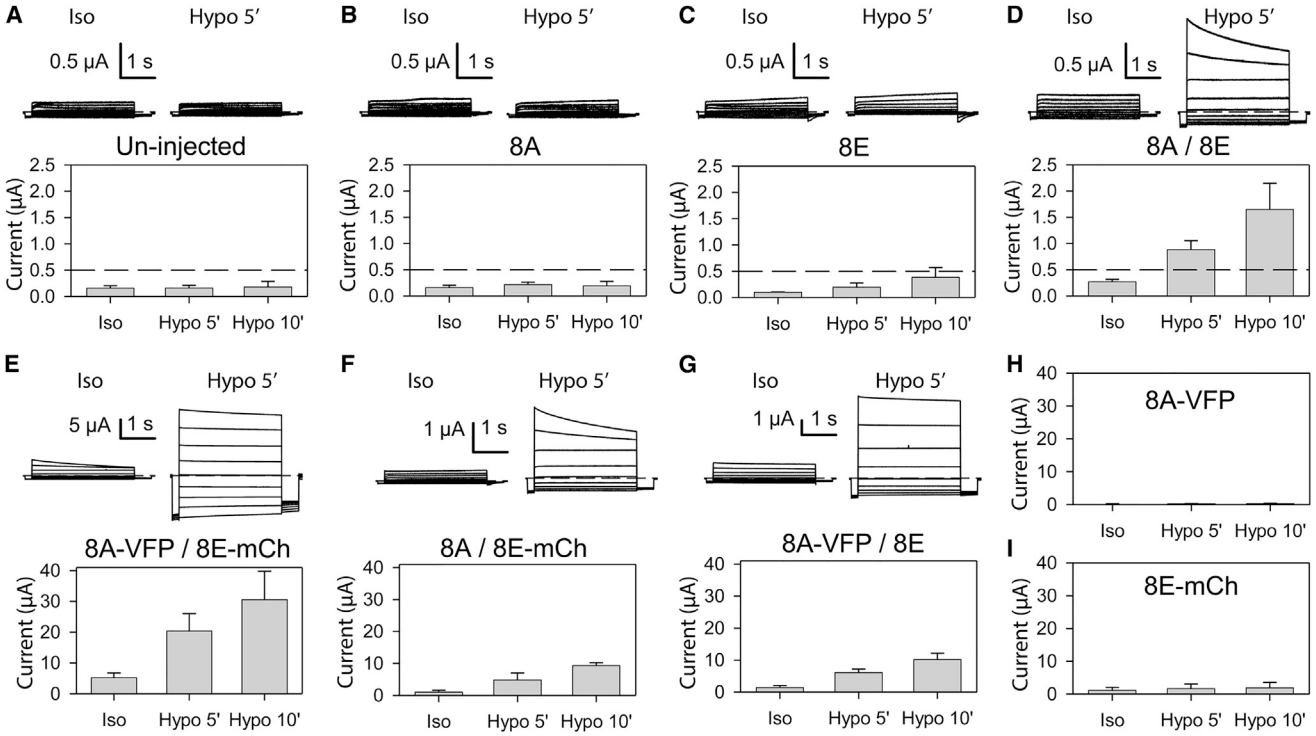

FIGURE 1 Functional expression of LRRC8-mediated VRAC currents in *Xenopus* oocytes. (*A*) Voltage-clamp traces of an uninjected oocyte evoked by the IV-pulse protocol in "Iso" (*A*, *top left*) and after 5 min perfusion of "Hypo" solution (*A*, *top right*). Mean values of currents at 60 mV from uninjected oocytes in "Iso," and after 5 min and 10 min in "Hypo" solution (*A*, *bottom*) ($n = 7$). (*B–G*, *top*) Currents of single oocytes injected with 8A (*B*) and 8E (*C*), and coinjected with 8A/8E (*D*), 8A-VFP/8E-mCherry (*E*), 8A/8E-mCherry (*F*), and 8A-VFP/8E (*G*) in response to the IV-pulse protocol in "Iso" solution and after 5 min perfusion with "Hypo" solution. (*B–G*, *bottom*) Current at 60 mV of 8A (*B*), 8E (*C*), 8A/8E (*D*), 8A-VFP/8E-mCherry (*E*), 8A/8E-mCherry (*F*), and 8A-VFP/8E (*G*) in "Iso" and after 5 min and 10 min in "Hypo" solution ($n \geq 4$). The dashed line in (*A*)–(*D*) indicates an arbitrary threshold of current expression corresponding to 0.5 μA. (*H* and *I*) Mean values of currents at 60 mV from oocytes injected with 8A-VFP (*H*) and 8E-mCherry (*I*) in "Iso" and after 5 min and 10 min in "Hypo" solution ($n \geq 4$). Error bars indicate the standard deviation.

and with similar kinetics and rectification of untagged volume stimulated 8A/8E-induced currents (Fig. 1 *D*). Importantly, 8A-VFP/8E-mCherry currents were strongly stimulated by hypotonicity (Fig. 1 *E*). In these conditions, the current magnitude caused series resistance problems resulting in an only apparent loss of the inactivating kinetics seen in isotonic conditions (Fig. 1 *E*).

We next tested coexpression of untagged constructs with tagged constructs. 8A/8E-mCherry (Fig. 1 *F*) and 8A-VFP/8E (Fig. 1 *G*) resulted in constitutively active currents in isosmotic conditions, which were strongly stimulated by hypotonicity but much smaller than 8A-VFP/8E-mCherry-induced currents (Fig. 1 *E*). Finally, we tested the expression of 8A-VFP and 8E-mCherry alone. 8A-VFP showed no significant currents even upon hypotonic stimulation (Fig. 1 *H*). However, 8E-mCherry exhibited small currents that increased upon hypoosmotic stimulation (Fig. 1 *I*) and after more days of expression (Fig. S4), but remained much smaller (<10%) than those of 8A-VFP/8E-mCherry (compare Fig. 1 *I* to Fig. 1 *E*, and see Fig. S4).

Coexpressing 8A fused with mCherry and 8E fused with VFP resulted in activation of currents similar to that for the inverse combination, and also, the coexpression of 8A-VFP with 8E-VFP or of 8A-mCherry with 8E-mCherry activated 8A/8E currents (Fig. S5). On the other hand, adding three copies of the flag epitope did not activate the currents, and adding three copies of the HA epitope led only to a very small activation (Fig. S5). Thus, the size of the added tags appears to be critical for a significant activation, although other factors, such as the charge or the shape of the tag, may also contribute.

We sought to test whether the constitutive activation of currents by adding fluorescent tags was specific for the proteins expressed in oocytes by patch clamping of 8A-VFP/8E-mCherry-transfected human embryonic kidney cells. However, we found this to be extremely difficult because of a very low success rate of giga-seal formation. In the few successful recordings, constitutive VRAC-like channel activity could be observed (data not shown). Because of this difficulty, we concentrated on the oocyte expression system.

Functional characteristics of the current induced by LRRC8 proteins

Based on the above described results, we exploited the fluorescently tagged subunits as a useful tool to investigate

several functional properties of the activity induced by LRRC8 proteins.

We prepared mCherry-labeled constructs for the other subunits (B, C, and D) and coexpressed these with 8A-VFP. All constructs were expressed in oocytes as shown by Western blot (Fig. S6), even though 8D-mCherry protein expression was much smaller than that of the other subunits (Fig. S6). The expression level of 8A was similar when expressed alone or coexpressed with the other subunits (Fig. S6 *A*). Differences in molecular weight between the subunits may be due to the variable presence of posttranslational modifications. Interestingly, 8A-VFP/8B-mCherry showed no significant currents even after 10 min of hypotonic stimulation (Fig. 2 *A*), although both subunits were expressed (Fig. S6). 8A-VFP/8C-mCherry resulted in large constitutive currents in isotonic conditions (Fig. 2 *B*), comparable to those for 8A-VFP/8E-mCherry (Fig. 2 *D*). Interestingly, 8A-VFP/8C-mCherry-induced currents exhibit no time-dependent inactivation at positive potentials (Fig. 2 *B*). 8A-VFP/8D-mCherry co-injection resulted in smaller constitutive and volume-stimulated currents compared to 8A-VFP/8E-mCherry (Fig. 2, *C* and *D*). At positive voltages, 8A-VFP/8D-mCherry (Fig. 2 *C*) displayed time-dependent inactivation kinetics similar to those of 8A-VFP/8E-mCherry (Fig. 2 *D*).

Taking advantage of the stable constitutive current exhibited by fluorescently tagged LRRC8 proteins in isotonic conditions, we could establish the selectivity sequence for various subunit combinations using reversal potential measurements as illustrated in Fig. S7. The permeability sequence found for 8A-VFP/8E-mCherry was $SCN^- > I^- > NO_3^- > Br^- > F^- > HCO_3^- >$ glycine > taurine > lactate > aspartate > gluconate > glutamate > Na^+. This is very similar to that previously found for VRACs (3) with a larger permeability to iodide than to chloride (Fig. 2 *E*, *left*). As already reported, this is an Eisenman anion sequence I ($I^- > Br^- > Cl^- > F^-$) corresponding to an anion binding site of weak field strength (3,6). 8A-VFP/8E-mCherry was instead substantially impermeable to Na^+ (P_{Na}/P_{Cl} ~2%), confirming that LRRC8 proteins are anion channels (Fig. 2 *E*, *left*). A very similar, but not identical, permeability sequence was found for 8A-VFP/8C-mCherry: $SCN^- > I^- > Br^- = NO_3^- > F^- >$ glycine > HCO_3^- > taurine > lactate > aspartate > gluconate = glutamate > Na^+ (Fig. 2 *E*, *middle*). Interestingly, the permeability sequence of 8A-VFP/8D-mCherry

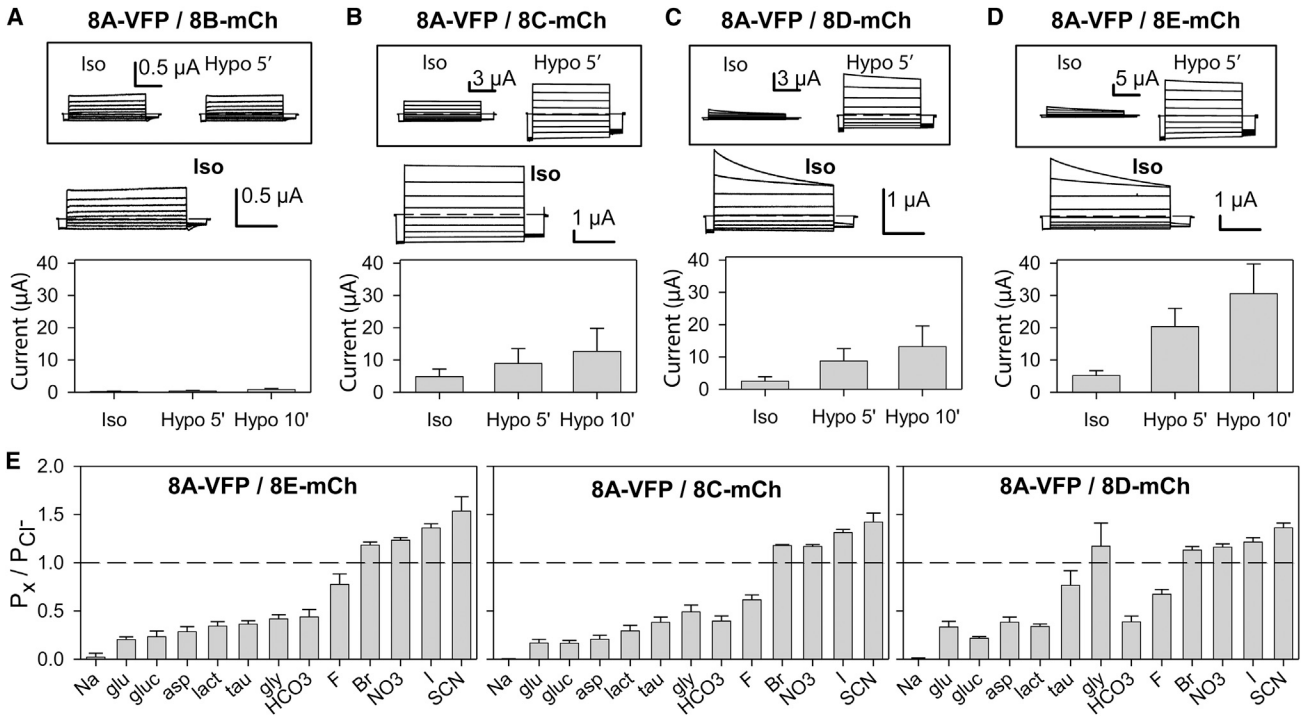

FIGURE 2 Inactivation and selectivity properties of VRAC currents mediated by different combinations of LRRC8 proteins. (*A–D*) Comparison of the current magnitude induced by co-expressing 8A-VFP with 8B-mCherry (*A*), 8C-mCherry (*B*), 8D-mCherry (*C*), and 8E-mCherry (*D*). Top: current traces from single oocytes evoked by the IV-pulse protocol in "Iso" solution (*left*) and after 5 min perfusion with "Hypo" solution (*right*). Middle: voltage clamp traces shown at higher magnification illustrate the typical relaxation kinetics. Horizontal bars: 1 sec; vertical bars: indicated in figure. Bottom: mean currents recorded in "Iso" solution, and after 5 min and 10 min in "Hypo" solution (n ≥ 4). (*E*) Permeation properties of hLRRC8A-VFP co-expressed with 8E-mCherry (*left*), 8C-mCherry (*middle*) and 8D-mCherry (*right*). Permeability ratios are estimated from the shifts in Erev caused by the substitution of Cl^- with glu, glutamate; gluc, gluconate; asp, aspartate; lact, lactate; tau, taurine; gly, glycine; HCO_3, bicarbonate; F, fluoride; Br, bromide; NO3, nitrate; I, iodide; SCN, thiocyanate, or Na^+ with TEA (n ≥ 4 for 8A-VFP/8E-mCherry; n ≥ 4; except for bicarbonate n = 3 for 8A-VFP/8C-mCherry; n ≥ 3 for 8A-VFP/8D-mCherry). The dashed line indicates the permeability for chloride. Primary data are shown in Fig. S7. Error bars indicate SD.

was $SCN^- > I^- >$ glycine $= NO_3^- > Br^- >$ taurine $> F^- > HCO_3^- =$ aspartate $>$ lactate $=$ glutamate $>$ gluconate $> Na^+$ (Fig. 2 *E*, *right*; Fig. S7 *C*). Thus, unlike 8C and 8E, the 8D-mCherry subunit confers a very large permeability to glycine (P_{gly}/P_{Cl} ~1.17) and taurine (P_{tau}/P_{Cl} ~0.76), suggesting that 8A-VFP/8D-mCherry is more efficient at transporting these substrates than the other heteromers, in agreement with recent published data (19).

Based on the large functional expression of 8A-VFP/8E-mCherry, we chose this heteromer to study single-channel properties of LRRC8-mediated currents. Single-channel measurements were performed on 8A-VFP/8E-mCherry-injected oocytes in the cell-attached configuration monitoring channel activity at potentials ranging from 80 to −80 mV. Typical recordings are shown in Fig. 3 *A*. In agreement with previous work on endogenous VRAC (5–7) and recent studies addressing LRRC8 reconstituted in bilayers (20), we found a pronounced outward rectification of the single-channel current-voltage relationship (Fig. 3, *A* and *B*), explaining the outward rectification of the macroscopic currents. At 80 mV, we measured a single-channel current $i = 2.57 \pm 0.29$ pA (chord conductance = 32 pS) (Fig. 3 *C*); at 20 mV, we found $i = 0.21 \pm 0.04$ pA (chord conductance = 11 pS); the conductance further decreased at negative potentials with $i = -0.37 \pm 0.06$ pA (chord conductance = 6 pS) at −60 mV (Fig. 3 *B*), which is very similar to what has been recently described (20), strongly indicating that the observed single-channel currents are mediated by LRRC8 proteins. Interestingly, the channels showed flickery openings at all voltages (Fig. 3 *A*).

Flux of organic osmolytes and ATP through LRRC8 proteins

Reversal potential measurements (Fig. 2 *E*) indicated that the expression of LRRC8 proteins induces a conductance that is permeable to amino acids such as glutamate and glycine as well as amino acid derivatives such as taurine.

To obtain additional independent evidence that these compounds can pass through LRRC8 proteins, we performed taurine, glutamate, and glycine radiotracer experiments. As the endogenous permeability for taurine and glutamate is very low (30,31), loading these substrates for efflux experiments would be rather difficult. However, we reasoned that influx experiments, although probably not in linear conditions, were feasible. We thus expressed 8A/8E and 8A-VFP/8E-mCherry and measured the uptake of radiolabeled taurine and glutamate after incubation in an isotonic or a hypotonic solution. In isotonic conditions, compared with uninjected oocytes, higher influx of radioactively labeled taurine (Fig. 4 *A*) and glutamate (Fig. 4 *B*) was observed in oocytes coexpressing untagged 8A and 8E, and it further increased in oocytes coexpressing 8A-VFP and 8E-mCherry. After incubation in a hypotonic solution, both groups showed high amounts of labeled taurine

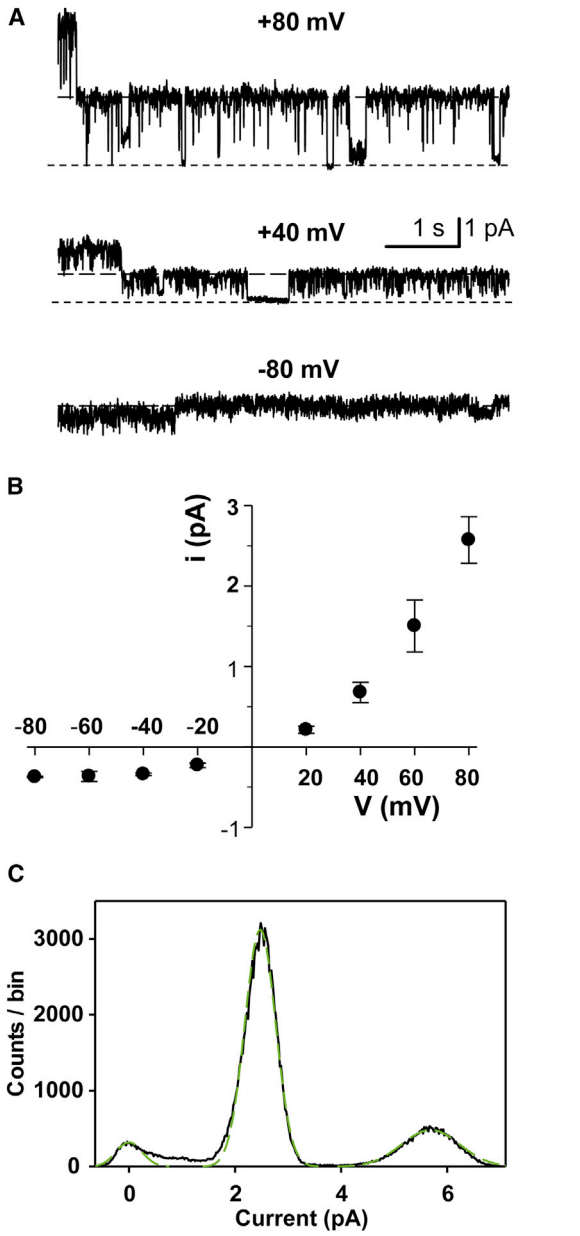

FIGURE 3 Single-channel studies of the 8A-VFP/8E-mCherry heteromer. (*A*) Representative traces from a cell-attached patch at 80, 40, and −80 mV. (*B*) Single-channel current-voltage relationship. Mean single-channel currents are plotted versus the corresponding potentials ranging between −80 and 80 mV. Note the outward rectification ($n \geq 4$) For −80, −40, and −20 mV, $n = 2$). Error bars indicate the standard deviation. (*C*) Amplitude histogram of the recording at 80 mV in control conditions. The dashed line represents the fit with a sum of three Gaussians. The dominant current level has an amplitude of 2.5 pA. To see this figure in color, go online.

(Fig. 4 *A*) and glutamate (Fig. 4 *B*). We analyzed the influx of taurine, glutamate, and glycine in isotonic (I) or hypotonic conditions (H) of 8A-VFP coexpressed with all the different subunits (8B, 8C, 8D, and 8E) tagged with mCherry. All heteromers except 8A-VFP/8B-mCherry showed influx of taurine (Fig. 4 *C*) and glutamate (Fig. 4 *D*). Also, glycine influx was significantly increased in tagged

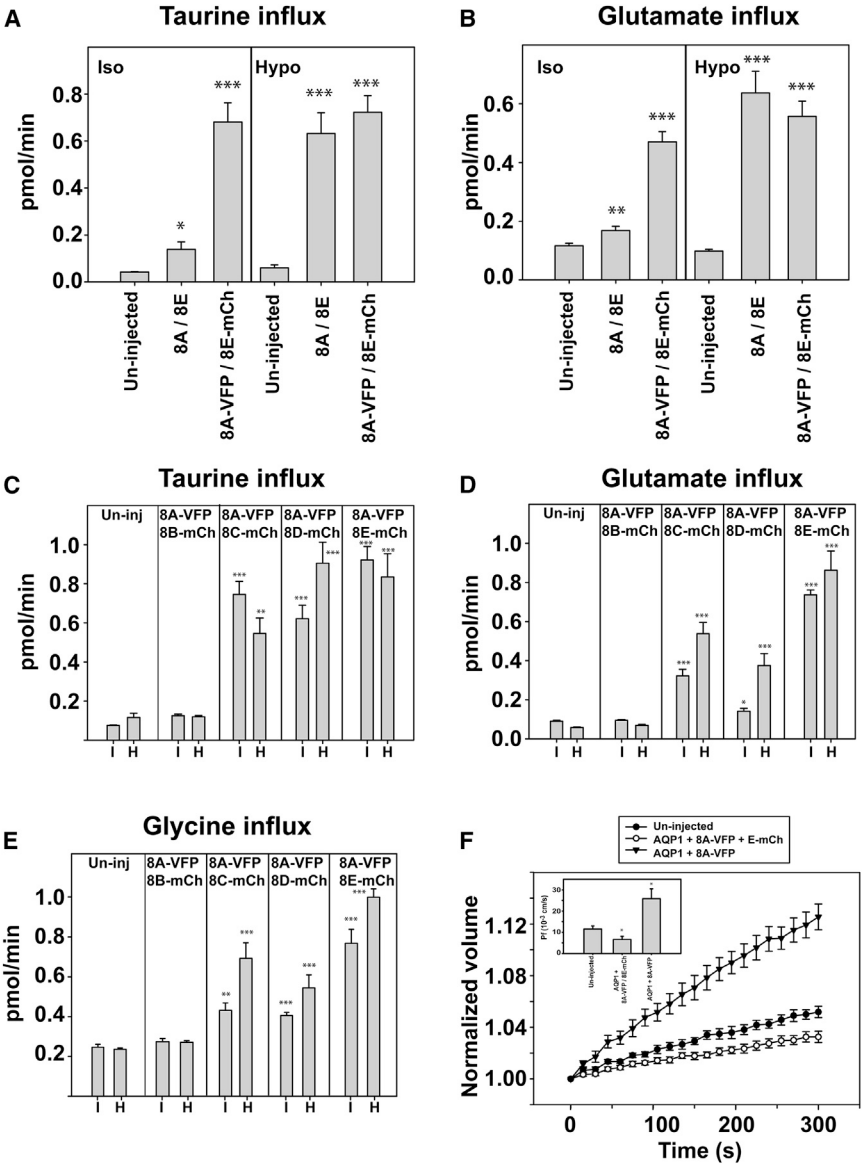

FIGURE 4 Uptake of osmolytes through LRRC8 proteins in *Xenopus* oocytes. (*A* and *B*) Comparison of the mean values of taurine (*A*) and glutamate (*B*) uptake between uninjected ($n \geq 6$) oocytes, oocytes injected with nontagged 8A/8E ($n \geq 5$) and oocytes injected with fluorescent-tagged 8A-VFP/8E-mCherry (n $\geq$ 6) in "Iso" solution (*left*) and "Hypo" solution (*right*). (*C–E*) Comparison of the mean values of taurine (*C*), glutamate (*D*), and glycine (*E*) uptake between uninjected oocytes and oocytes injected with 8A-VFP co-expressed with 8B-mCherry, 8C-mCherry, 8D-mCherry, and 8E-mCherry ($n \geq 3$ for all co-expressions) in Iso "I" and Hypo "H" solution. (*F*) Time course of normalized oocyte volume in ND48 solution and apparent water permeability mean values (*inset*) of uninjected oocytes ($n = 6$), AQP1 + 8A-VFP ($n = 8$), and AQP1 + 8A-VFP/8E-mCherry ($n = 10$) injected oocytes. Data indicate the mean ± SE. $^*p < 0.05$, $^{**}p < 0.01$, $^{***}p < 0.001$.

8A/8C-, 8A/8D-, and 8A/8E-coexpressing, but not 8A/8B-coexpressing oocytes in isotonic and even more in hypotonic conditions (Fig. 4 *E*). However, the difference to noninjected oocytes was smaller compared to that seen for taurine and glutamate influx (Fig. 4, *C–E*).

The release of osmolytes, especially taurine, through the VRAC channel is important for the process of RVD induced by swelling (4). *Xenopus* oocytes show low water permeability, reflecting the lack of aquaporins and the lipid composition of the membrane (32). Water permeability can be dramatically increased by the expression of aquaporin-1 (AQP1) such that hypotonic exposure leads to oocyte swelling and membrane disruption (32). To test whether LRRC8 proteins are able to protect oocytes from such cell swelling, we coexpressed AQP1 with 8A-VFP/8E-mCherry. Indeed, swelling was dramatically reduced and was even lower than that seen in oocytes without AQP1 (Fig. 4 *F*). To rule out that RNA competition nonspecifically reduced AQP1 expression in coinjected oocytes, we coinjected AQP1 with 8A-VFP RNA alone (at the same amount) and found that hypotonic challenge resulted in pronounced oocyte swelling (Fig. 4 *F*), suggesting that AQP1 activity is not affected by RNA competition.

Another substrate previously suggested to be transported through VRACs is ATP (33). To test whether LRRC8 proteins are able to promote ATP release, we first measured ATP efflux under hypotonic exposure (15 mOsm) for the 8A/8E and 8A-VFP/8E-mCherry combinations using a luciferase-based assay. We found that ATP release increased with time after hypotonic stimulation in 8A/8E-expressing oocytes, and even more so in 8A-VFP/8E-mCherry-expressing oocytes, but not in uninjected oocytes (Fig. 5, *A* and *B*).

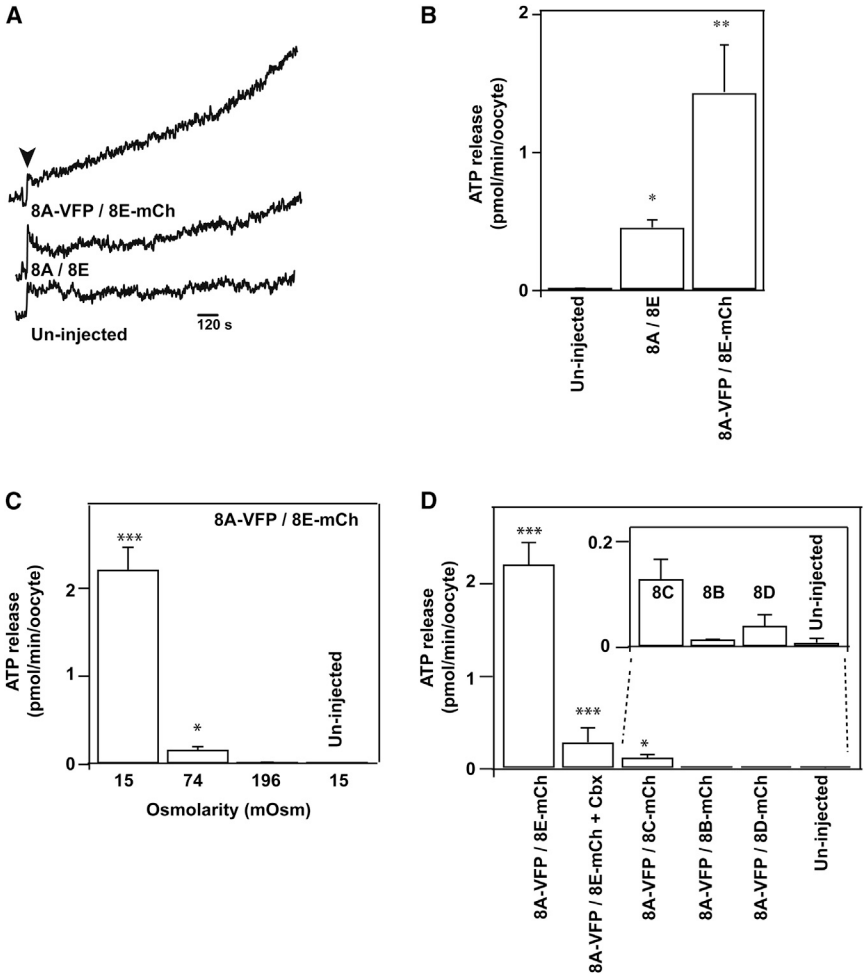

FIGURE 5 ATP release through LRRC8 proteins. (*A*) ATP-release representative traces of uninjected oocytes (*bottom*), oocytes injected with 8A/8E (*middle*), and oocytes injected with 8A-VFP/8E-mCherry (*top*). The black arrowhead indicates the beginning of the hypotonic exposure (15 mOsm). (*B*) Amount of ATP released (pmol/oocyte/min) from uninjected oocytes ($n = 4$), oocytes injected with 8A/8E ($n = 5$) and oocytes injected with 8A-VFP/8E-mCherry ($n = 5$). (*C*) Amount of ATP released from oocytes injected with 8A-VFP/8E-mCherry incubated in solutions with different osmolarities, 15 ($n = 6$), 74 ($n = 4$), and 196 ($n = 4$) mOsm, or from uninjected oocytes at 15 mOsm ($n = 4$). (*D*) Amount of ATP released in hypotonic conditions from oocytes injected with 8A-VFP/8E-mCherry ($n = 6$), 8A-VFP/8E-mCherry in the presence of 100 μM CBX ($n = 5$), 8A-VFP/8C-mCherry ($n = 4$), 8A-VFP/8B-mCherry ($n = 4$), 8A-VFP/8D-mCherry ($n = 4$), and uninjected oocytes ($n = 4$). Data indicate the mean ± SE. $^{*}p < 0.05$, $^{**}p < 0.01$, $^{***}p < 0.001$.

ATP release strongly depended on osmolarity (Fig. 5 *C*) and was blocked by CBX (Fig. 5 *D*). Finally, we analyzed ATP release in oocytes coexpressing 8A-VFP with other mCherry-tagged subunits (B, C, and D). A much smaller but significant ATP release was observed for 8A-VFP/8C-mCherry, whereas it was not statistically significant in heteromers containing tagged 8B or 8D (Fig. 5 *D*, *inset*). These results suggest that ATP permeates better through 8A/8E channels than through 8A/8C channels. We thus tested whether ATP differently affects the currents mediated by these subunit combinations. However, addition of 1 mM ATP blocked by ~50% both 8A-VFP/8E-mCherry- and 8A-VFP/8C-mCherry-mediated currents (data not shown).

Mechanism of CBX inhibition of LRRC8-mediated currents

We next aimed to characterize the mechanism of CBX inhibition of LRRC8-mediated currents. CBX is the succinyl ester of glycyrrhizic acid that was shown previously to inhibit VRAC currents (10) and recently also LRRC8-mediated currents (17). Therefore, we tested CBX on 8A-VFP/8E-mCherry-induced currents at various concentrations from 10 to 500 μM (Fig. 6 *A*). Increasing [CBX] resulted in increasing block of the currents. For low [CBX], complete steady-state inhibition was difficult to achieve in reasonable recording times (Fig. 6 *A*). Thus, to estimate steady-state block, we fitted an exponential function to the time course of the onset of block and extrapolated it to infinite time (Fig. 6 *A*, *solid lines*). Using this procedure, we found ~59% residual current at 10 μM CBX and only ~7% at 100 μM CBX. The residual currents at 500 μM CBX were at the level of endogenous currents, indicating that block is practically complete at high [CBX]. We fitted the CBX block by a simple binding curve (see Materials and Methods). The best fit yields an apparent affinity constant (K_A) of 11.9 μM and a Hill coefficient (n) of 1.8 (Fig. 6 *B*, *red line*). The Hill coefficient of 1.8 suggests that more than one CBX molecule is required to block the channel. In fact, fixing the Hill coefficient at 1 yields a poor fit to the data (Fig. 6 *B*, *black dashed line*). However, since the experiments were performed without washout control, further evidence is needed to draw a firm conclusion on the number of CBX binding sites.

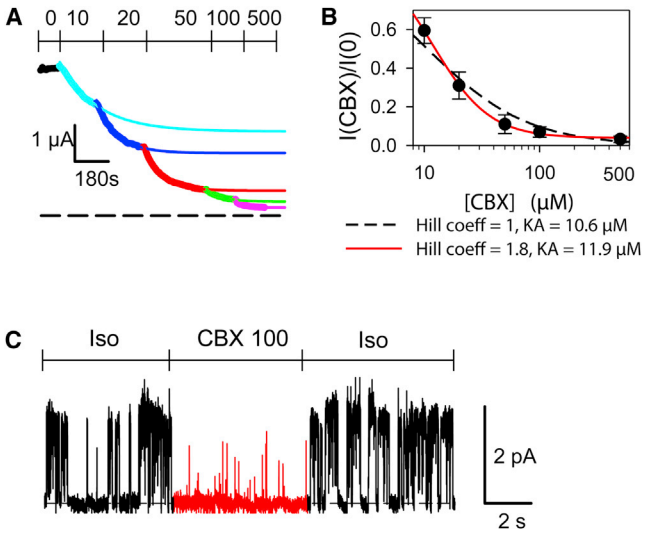

FIGURE 6 Carbenoxolone inhibition of 8A-VFP/8E-mCherry. (*A*) Currents recorded in voltage clamp at 60 mV are plotted as function of the time. Colors correspond to the different CBX concentrations (10, 20, 50, 100, 500 μM) applied during the experiment. In order to estimate the steady-state effect, single-exponential functions were fitted to the time course and extrapolated to infinite time (*solid colored lines*). (*B*) Concentration dependence of CBX modulation of hLRRC8A-VFP/8E-mCherry. Currents acquired at 60 mV are normalized to values measured in "Iso" solution and plotted versus CBX concentrations. The red line represents the best fit of hLRRC8A-VFP/8E-mCherry currents (fit parameters: Hill coefficient = 1.8, KA = 11.9 μM, $p_\infty = 0.038$), while the black dashed line (fit parameters: Hill coefficient = 1.0, KA = 10.6 μM, $p_\infty = 0$) poorly fits the data. These theoretical predictions are obtained using Eq. 3 as described in Methods. ($n \geq 8$, except for 50 μM, where $n = 4$). (*C*) Representative trace from an outside-out patch at 80 mV in "Iso" solution (*black*), 100 μM CBX (*red*), and wash in "Iso" solution (*black*). Error bars indicate SD. To see this figure in color, go online.

In voltage-clamp measurements, CBX blocked LRRC8 induced currents when applied from the extracellular side (Fig. 6 *A*). However, washout of the CBX effect was rather slow and we could not exclude the possibility that the relatively hydrophobic molecule crosses the plasma membrane and exerts its blocking effect from the inside. We thus performed patch-clamp experiments in the outside-out configuration to test whether CBX acts directly from the outside. Application of 100 μM CBX on the excised patch resulted in an almost immediate channel closure (Fig. 6 *C*). This block was quickly reversed upon washout of CBX (Fig. 6 *C*). For the outside-out patch-clamp experiments, we estimated ~18% residual current in the presence of CBX, which is slightly larger compared to the effect in two-electrode voltage clamp. In any case, the rapid onset of block and the almost immediate recovery upon wash strongly suggest that the CBX binding site is exposed to the extracellular side.

Counting subunits in LRRC8 heteromers

Bioinformatic analyses have revealed a phylogenetic relation of LRRC8 proteins to pannexins (34). Experimental evidence based on cross-linking and native gels suggests that pannexins may form hexameric complexes (35), although other studies suggest that pannexin-2 may assemble into heptamers or octamers (36). Recent cross-linking studies suggest that also, LRRC8 complexes may contain six to eight subunits (20). However, pannexins are homomeric (37), whereas LRRC8 channels are multimeric complexes of LRRC8A and other LRRC8 members (17).

To obtain insight into the stoichiometry of LRRC8 channels, we used TIRF microscopy to visualize the fluorescently tagged subunits in the membrane at single-particle resolution. When 8A-VFP was injected alone, we observed a variable but overall large number of diffraction-limited spots (150 $\pm$ 30 spots/field of view (FOV), $n = 3$ FOVs). For 8E-mCherry alone, the number of spots was much smaller (21 $\pm$ 13 spots/FOV, $n = 4$). Upon coexpression of 8A-VFP with 8E-mCherry, the number of 8E-mCherry spots significantly increased (42 $\pm$ 16 spots/FOV, $n = 11$, $p = 0.004$), whereas the number of 8A-VFP spots slightly decreased (83 $\pm$ 24 spots/FOV, $n = 11$). Twenty-six percent of the 8A-VFP spots colocalized with 8E-mCherry spots, and 51% of 8E-mCherry spots colocalized with the 8A-VFP spots ($n = 11$, $p = 0.003$) (Fig. 7 *A*). These results suggest that 8A and 8E form oligomeric complexes at the plasma membrane, that 8E relies on 8A to achieve efficient plasma membrane expression, as previously reported (17), and that 8A levels at the plasma membrane are independent of 8E.

To investigate whether more than two different subunits may be associated in the same complex, we coexpressed untagged 8A with 8E-VFP and 8D-mCherry and detected colocalization of 8E-VFP and 8D-mCherry (Fig. S8 *A*). Assuming that 8A is obligatorily present, this indicates that LRRC8 complexes may be formed by more than two different subunits.

Since the tagged subunits were relatively immobile in the oocyte membrane, we used single-step photobleaching to count and estimate the number of subunits within the hetero-oligomers. This method has been used to determine the stoichiometry of small oligomers (five to six subunits) (24,38). For an oligomer with fixed stoichiometry, the distribution of the observed number of photobleaching steps is binomial, whereas for a variable stoichiometry the distribution is expected to be Poissonian (see Materials and Methods).

We extracted intensity-time traces from 8A-VFP particles that colocalized with 8E-mCherry particles and thus were heteromeric (Fig. 7 *B*). The number of photobleaching steps showed a broad distribution (Fig. 7 *C*) and we could reliably count only up to six photobleaching steps, since for more than six steps, the probability of multiple fluorescent proteins photobleaching simultaneously increases (Fig. S8 *B*). This broad distribution is not compatible with a binomial distribution assuming 80% probability for VFP to be fluorescent and a fixed stoichiometry ranging from 1 to 6

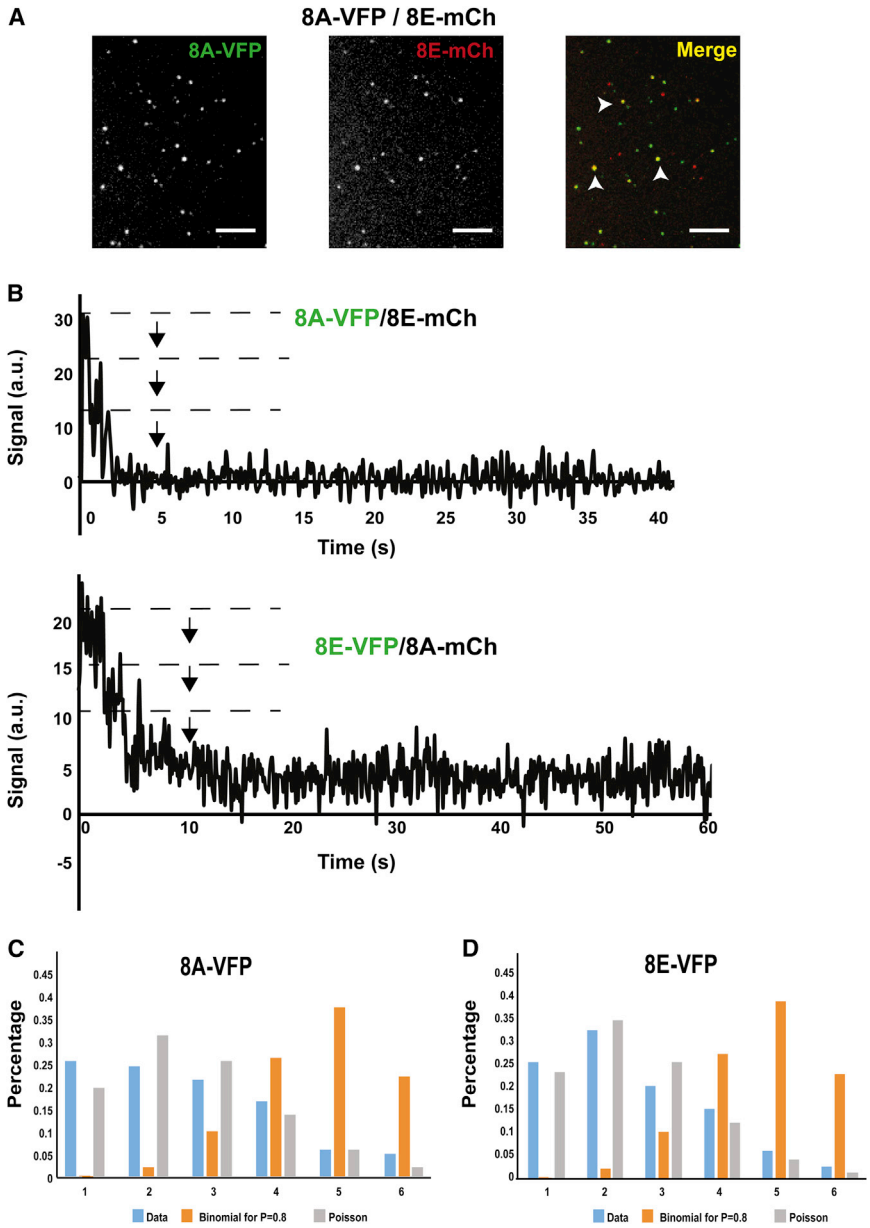

FIGURE 7 Subunit counting of LRRC8 heteromers by single-step photobleaching. (*A*) TIRF image showing LRRC8A-VFP and LRRC8E-mCherry oligomers on the Xenopus oocyte membrane and a merge of the two fluorescent channels. Arrowheads point to overlapping LRRC8A and LRRC8E spots. Scale bar: 5 μm. (*B*) Intensity-time traces showing individual photobleaching steps from one of the LRRC8A-VFP oligomers in complex with LRRC8E-mCherry (*upper*) or the LRRC8E-VFP oligomers in complex with LRRC8A-mCherry (*lower*) identified on the oocyte membrane in TIRF microscopy. Dashed lines and arrows indicate observed single steps. (*C*) Distribution of the percentage of counted steps ($n = 142$) from LRRC8A-VFP oligomers in complex with LRRC8E-mCherry oligomers at equimolar ratio. (*D*) Distribution of the percentage of counted steps ($n = 158$) from LRRC8E-VFP oligomers in complex with LRRC8A-mCherry oligomers at equimolar ratio. Blue bars in C and D indicate the data, orange bars show the prediction of a binomial distribution (Eq. 4) with $P = 0.8$ and gray bars indicate the best fits of Poisson distribution (Eq. 5). To see this figure in color, go online.

(Fig. 7 *C*). Instead, it fits well to a Poisson distribution (Fig. 7 *C*), indicating that the number of 8A subunits present in LRRC8 hetero-oligomers is variable. We calculated an average number of ~3 8A-subunits within the hetero-oligomers. As this number is very similar to what has been observed recently in cross-linking experiments (20), we assume that we are predominantly measuring fluorescence from a single VRAC channel and not from clusters of channels.

To similarly determine the number of 8E subunits in the hetero-oligomers, we injected an equimolar ratio of 8E-VFP and 8A-mCherry and extracted intensity-time traces from 8E-VFP spots that colocalized with 8A-mCherry spots (Fig. 7 *B*). The expression level of the two subunits was similar to that of the 8A-VFP/8E-mCherry combination (70 ± 22 8A-mCherry spots and 49 ± 27 8E-VFP spots/FOV, $n = 9$). In addition, the percentage of colocalization between 8A-mCherry and 8E-VFP was similar (28% of 8A-mCherry colocalized with 8E-VFP and 38% of 8E-VFP colocalized with 8A-mCherry; $n = 9$). As for 8A-VFP (Fig. 7 *C*), we observed a broad distribution for the number of photobleaching steps that fits well with a Poisson distribution (Fig. 7 *D*), with an average of ~2.5 subunits (Fig. 7 *D*). Taken together, these results suggest that the number of 8A and 8E subunits in LRCC8 hetero-oligomers is variable and that on average the total number of subunits is >5. We note that since the folding of VFP is incomplete but high (~80%), the number of subunits may be slightly underestimated.

It has been reported that overexpression of LRRC8A decreased VRAC currents in a manner similar to that

observed in the inhibition by RNA interference (16,17). Given that in *Xenopus* oocytes it is very easy to change the relative expression of each subunit by changing the amount of injected cRNA, we compared the currents induced by injection of equimolar amounts of 8A-VFP and 8E-mCherry (1:1) with those induced by increasing the relative amount of 8A-VFP versus 8E-mCherry (3:1) (Fig. S8 *C*). Increasing the relative amount of 8A-VFP decreased the currents by ~75–80% (Fig. S8 *C*, *left*), with similar results for 8A-mCherry and 8E-VFP (Fig. S8 *C*, *right*). We also counted the number of photobleaching steps for 8A-VFP when the ratio was 3:1 and found an average number of ~4 A-subunits in the complex, indicating that the stoichiometry of each LRRC8 protein is not fixed but likely depends on their relative abundance (Fig. S8 *D*).

Fluorescent-tagged LRRC8 proteins show a shift in their osmolarity dependence

Physiologically, VRAC is closed under isotonic conditions, and indeed, oocytes injected with wild-type 8A/8E or 8A/8D subunits do not show significant currents in isotonic conditions (Fig. 1; Fig. S1). Thus, the constitutive currents induced by the fluorescently tagged LRRC8 proteins in isosmotic conditions raise the question of whether the tags render the channels constitutively open or they are still able to close. To address this question, we studied in quantitative detail the dependence of 8A-VFP/8E-mCherry-induced currents on the extracellular osmolarity.

Interestingly, the constitutively active currents seen after expression of the fluorescently tagged subunits are reduced by application of a hyperosmotic solution (310 mOsm) to <20% (Fig. 8). This result indicates that the addition of the fluorescent tags leads to a "shift" of the osmosensitivity of the channels such that a basal activation is present even under isotonic conditions. Decreasing the osmolarity to 120 mOsm leads to a ninefold activation of 8A-VFP/8E-mCherry-mediated currents compared to the isotonic solution, whereas further osmolarity reductions (to 74 and 40 mOsm) result in 17-fold and 25-fold current increases, respectively (Fig. 8). Thus, the osmolarity dependence of these channels is not even saturated at 40 mOsm (Fig. 8, *right*). Because the untagged constructs responded more slowly to hypotonic challenges, it was unfeasible to assay their osmosensitivity in a similar manner.

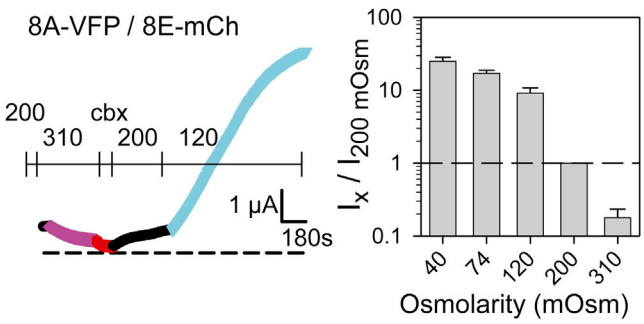

FIGURE 8 Osmolarity dependence of 8A-VFP/8E-mCherry. Left: currents at 60 mV are plotted vs. time. Colors correspond to the different extracellular osmolarities applied (200, 310, 120 mOsm); additionally, CBX was applied to test the endogenous current contribution. Right: quantification of the osmolarity dependence of 8A-VFP/8E-mCherry. Currents at 60 mV recorded at osmolarity values between 40 and 310 mOsm are normalized to the currents measured in "Iso" solution (200 mOsm). Error bars indicate SD ($n \leq 5$). To see this figure in color, go online.

DISCUSSION

VRAC currents mediate RVD in many cells and thus play an important physiological role (3). After a long search for the molecular correlates of VRACs (15), finally two independent groups identified LRRC8 proteins as major constituents of the VRAC channel (16,17). However, even after the successful identification, the investigation of the properties of the channel remained challenging, requiring knock-out cell lines for heterologous expression (17,18,20). Here, we show that a simple approach (C-terminal tagging by fluorescent proteins) resulted in constitutive open channels of large magnitude. This allowed investigation of the functional properties of the currents induced by LRRC8 proteins in *Xenopus* oocytes. Using this system, we could confirm previous suggestions that VRAC is able to create a path for many anions and osmolytes, including taurine, glutamate, glycine, and ATP (3,5,39). We could detect significant ATP release for the heteromers 8A-VFP/8E-mCherry and 8A-VFP/8C-mCherry. ATP release was not detected for 8A-VFP/8D-mCherry, probably due to the lower expression of this heteromer in the oocyte system. Expression of LRRC8A alone together with AQP1 has been previously shown to induce chloride currents in oocytes (40). However, we believe that these currents could be due to indirect effects on endogenous currents, as they were also observed when expressing the unrelated membrane protein anoctamin 10 together with AQP1 (40). In our study, LRRC8A alone never gave rise to any significant currents.

Several pieces of evidence support the conclusion that the activity measured in our experiments is due to the expression of the exogenous proteins. 1) As already described in cell lines (17–19), we observed differences in inactivation and selectivity properties for different LRRC8 heteromers. Moreover, single-channel analyses at different voltages were in agreement with previous studies of the VRAC current (3,7) and what has been observed in bilayers after LRRC8 reconstitution (20). 2) We could observe flux of radioactive taurine, glutamate, and glycine, whereas uninjected oocytes have negligible flux for taurine and glutamate and less flux for glycine. 3) Currents were blocked by CBX (10). It has to be considered that VRAC currents have been previously observed in manually isolated *Xenopus* oocytes, but never in collagenase-treated oocytes, as we also confirmed (8,29). It has been suggested that the

VRAC channel might be present in the follicle cells but not in the oocyte membrane (28). We envisage that the endogenous LRRC8 proteins are kept in a dormant state, as has been found in other channels or transporters (41,42). Only by injecting large amounts of LRRC8E-mCherry RNA and after several days could we observe VRAC-like currents. However, compared to the current induced by coexpressing LRRC8A-VFP with LRRC8E-mCherry, the current induced by LRRC8E-mCherry alone was very small (<10%). Thus, a possible endogenous background can be rather safely neglected.

Phylogenetic analyses suggested that the LRRC8 protein family evolved from an ancestral pannexin protein in chordates (34). This homology can clearly be observed via the conservation of cysteine residues in extracellular loops, which are also present in connexins (43). Recently, the first extracellular loop of pannexin1 was found to be involved in CBX binding (13), in agreement with our finding that CBX blocks LRRC8-mediated currents acting extracellularly. This evolutionary relationship also suggested that LRRC8 proteins might form hexameric complexes (37). Our results using single-step photobleaching suggest that the total number of subunits (LRRC8A plus LRRC8E) on average is >5. Since the method relies on counting inactivation steps of VFP, it is challenging to estimate stoichiometry when the number of subunits is very high. However, we found that, when expressed at equimolar levels, the average numbers of LRRC8A and LRRC8E subunits are similar. It will be interesting to find out whether LRRC8A and LRRC8E subunits occupy segregated parts of the heteromer or are interdigitated. Our data further suggest that the complex might contain more than two different LRRC8 subunits. In addition, we found that the stoichiometry is likely not fixed, since the distribution of the number of bleaching steps did not follow a binomial distribution and because the distribution changed upon altering the relative amount of each subunit. Thus, we hypothesize that the dominant negative functional effects observed by the overexpression of LRRC8A may be caused by the formation of nonfunctional stoichiometries. Similar dominant negative effects are observed when overexpressing nicotinic receptors (44), probably by having complexes of nonnative stoichiometries. Thus, we envisage that changing the relative proportion of each subunit may be a way to regulate VRAC channel activity. In this regard, it is interesting to note that heterologous coexpression of LRRC8A and LRRC8B subunits does not result in functional activity (this work and (17)), although the proteins are located at the plasma membrane (17). However, cells expressing only endogenous LRRC8A and LRRC8B (knock-out of LRCC8C/D/E) exhibit VRAC currents (17). It may be that heteromers containing LRRC8B need a stimulus to be active, or, alternatively, LRRC8B could work as an inhibitory subunit.

Many different mechanisms, such as oxidation, phosphorylation, ionic strength, intracellular Na^+ concentration, changes in subcellular localization, and membrane or cytoskeleton stretch (3,6,14,15,20,45–47), have been proposed to regulate the activity of VRAC channels. Here, we found that the addition of fluorescent proteins to the C-terminus, which contains the leucine-rich repeats (48), resulted in constitutively active channels, which are, however, further activated by hypotonicity and inhibited by hypertonicity. We thus suggest that some of the mechanisms known to regulate channel activity may influence the conformation of the C-terminus. In a similar manner, one of the proposed mechanisms for pannexin-1 activation involves the C-terminus, which can be cleaved by caspase, and which could act as a plug in the transmembrane pore (49–52). Further studies are needed to determine whether this mechanism is also occurring in LRRC8 proteins.

In summary, our work established the *Xenopus* oocyte system as a valid expression system for LRRC8 proteins, and it describes, to our knowledge, new characteristics of this channel. We consider the oocyte system as a complementary approach to the expression in knockout cell lines (17). The oocyte system offers the advantage of the possibility of performing a variety of electrophysiological, optical, and biochemical assays on single cells (53–55) with the ability to control the expression of each subunit independently. Furthermore, the constitutive channel activity in physiological conditions observed after C-terminal fusion of fluorescent proteins in oocytes could facilitate drug screening of this channel. We envisage that the easiness of the oocyte system described here, combined with the activation conferred by the addition of the fluorescent proteins, could be crucial to discover novel structure-function relationships of the VRAC channel formed by LRRC8 proteins. We believe that our system also will be helpful in the unraveling of molecular determinants of novel physiological and pathophysiological roles of LRRC8 proteins, as, for example, their involvement in chemotherapeutic drug resistance (19).

SUPPORTING MATERIAL

Eight figures are available at http://www.biophysj.org/biophysj/supplemental/S0006-3495(16)30752-4.

AUTHOR CONTRIBUTIONS

The present project was initiated at the lab of R.E. Functional 2-EV electrophysiological measurements were done in the lab of M.P. and R.E. by A.G. and H.G-P., and single-channel studies were done by A.G. and M.P. H.G-P, L.L-C., R.E., and M.L. performed TIRF and step-bleaching experiments and analyses. H.G-P., R.E., and C.S. performed ATP experiments. H.G-P and R.E. performed radioactive uptake and volume measurement experiments. V.F-D and F.C. helped in the design of experiments. All authors planned and analyzed experiments. R.E. and M.P. supervised experiments. R.E. and M.P were the primary writers and managed production of the manuscript with critical input from all the authors, who read and provided feedback on the manuscript.

ACKNOWLEDGMENTS

This study was supported by the European Leukodystrophies Association (ELA) Research Foundation (ELA2012-014C2B), Ministerio de Ciencia e Innovación (MICINN) (SAF 2012-31486 and SAF 2015-70377), Generalitat de Catalunya (SGR2014-1178), and Istituto de Salud Carlos III (ISCIII, ERARE) to R.E and by the Italian Telethon Foundation (grant GGP12008) to M.P. R.E. was awarded Icrea Academia prizes (2009 and 2014). M.L. acknowledges financial support from the Ministry of Economy and Competitiveness (MINECO) through the "Severo Ochoa" Programme for Centres of Excellence in R&D (SEV-2015-0522), a Severo Ochoa PhD fellowship to L.L-C., Fundació Privada Cellex, the European Union Seventh Framework Programme under European Research Council grant 337191-MOTORS, and the Spanish Ministry of Economy and Competitiveness (MINECO) and the "Fondo Europeo de Desarrollo Regional" (FEDER) through grant FIS2012-37753. F.C. acknowledges financial support from MINECO/ISCIII (grants SAF2014-55700-P, PCIN-2013-019-C03-03 and PIE14/00034) and the Agency for Innovation in Science and Technology (IWT) (SBO-140028).

REFERENCES

1. Hoffmann, E. K., I. H. Lambert, and S. F. Pedersen. 2009. Physiology of cell volume regulation in vertebrates. *Physiol. Rev.* 89:193–277.
2. Pasantes-Morales, H., and S. Cruz-Rangel. 2010. Brain volume regulation: osmolytes and aquaporin perspectives. *Neuroscience.* 168:871–884.
3. Pedersen, S. F., Y. Okada, and B. Nilius. 2016. Biophysics and physiology of the volume-regulated anion channel (VRAC)/volume-sensitive outwardly rectifying anion channel (VSOR). *Pflugers Arch.* 468:371–383.
4. Manolopoulos, V. G., T. Voets, …, B. Nilius. 1997. Swelling-activated efflux of taurine and other organic osmolytes in endothelial cells. *Am. J. Physiol.* 273:C214–C222.
5. Nilius, B., J. Eggermont, …, G. Droogmans. 1997. Properties of volume-regulated anion channels in mammalian cells. *Prog. Biophys. Mol. Biol.* 68:69–119.
6. Pedersen, S. F., T. K. Klausen, and B. Nilius. 2015. The identification of a volume-regulated anion channel: an amazing Odyssey. *Acta Physiol. (Oxf.).* 213:868–881.
7. Jackson, P. S., and K. Strange. 1996. Single channel properties of a volume sensitive anion channel: lessons from noise analysis. *Kidney Int.* 49:1695–1699.
8. Decher, N., H. J. Lang, …, K. Steinmeyer. 2001. DCPIB is a novel selective blocker of I(Cl,swell) and prevents swelling-induced shortening of guinea-pig atrial action potential duration. *Br. J. Pharmacol.* 134:1467–1479.
9. Minieri, L., H. Pivonkova, …, S. Ferroni. 2013. The inhibitor of volume-regulated anion channels DCPIB activates TREK potassium channels in cultured astrocytes. *Br. J. Pharmacol.* 168:1240–1254.
10. Benfenati, V., M. Caprini, …, S. Ferroni. 2009. Carbenoxolone inhibits volume-regulated anion conductance in cultured rat cortical astroglia. *Channels (Austin).* 3:323–336.
11. de Pina-Benabou, M. H., V. Szostak, …, R. Rozental. 2005. Blockade of gap junctions in vivo provides neuroprotection after perinatal global ischemia. *Stroke.* 36:2232–2237.
12. Frantseva, M. V., L. Kokarovtseva, …, J. L. Perez Velazquez. 2002. Specific gap junctions enhance the neuronal vulnerability to brain traumatic injury. *J. Neurosci.* 22:644–653.
13. Michalski, K., and T. Kawate. 2016. Carbenoxolone inhibits Pannexin1 channels through interactions in the first extracellular loop. *J. Gen. Physiol.* 147:165–174.
14. Jentsch, T. J., D. Lutter, …, F. K. Voss. 2016. VRAC: molecular identification as LRRC8 heteromers with differential functions. *Pflugers Arch.* 468:385–393.
15. Stauber, T. 2015. The volume-regulated anion channel is formed by LRRC8 heteromers—molecular identification and roles in membrane transport and physiology. *Biol. Chem.* 396:975–990.
16. Qiu, Z., A. E. Dubin, …, A. Patapoutian. 2014. SWELL1, a plasma membrane protein, is an essential component of volume-regulated anion channel. *Cell.* 157:447–458.
17. Voss, F. K., F. Ullrich, …, T. J. Jentsch. 2014. Identification of LRRC8 heteromers as an essential component of the volume-regulated anion channel VRAC. *Science.* 344:634–638.
18. Ullrich, F., S. M. Reincke, …, T. J. Jentsch. 2016. Inactivation and anion selectivity of volume-regulated VRAC channels depend on carboxy-terminal residues of the first extracellular loop. *J. Biol. Chem.* 291:17040–17048.
19. Planells-Cases, R., D. Lutter, …, T. J. Jentsch. 2015. Subunit composition of VRAC channels determines substrate specificity and cellular resistance to Pt-based anti-cancer drugs. *EMBO J.* 34:2993–3008.
20. Syeda, R., Z. Qiu, …, A. Patapoutian. 2016. LRRC8 Proteins form volume-regulated anion channels that sense ionic strength. *Cell.* 164:499–511.
21. Hille, B. 2001. Ion channels of excitable membranes. Sinauer, Sunderland, Mass.
22. Duarri, A., O. Teijido, …, R. Estévez. 2008. Molecular pathogenesis of megalencephalic leukoencephalopathy with subcortical cysts: mutations in MLC1 cause folding defects. *Hum. Mol. Genet.* 17:3728–3739.
23. Durisic, N., A. G. Godin, …, J. A. Dent. 2012. Stoichiometry of the human glycine receptor revealed by direct subunit counting. *J. Neurosci.* 32:12915–12920.
24. Durisic, N., L. Laparra-Cuervo, …, M. Lakadamyali. 2014. Single-molecule evaluation of fluorescent protein photoactivation efficiency using an in vivo nanotemplate. *Nat. Methods.* 11:156–162.
25. McGuire, H., M. R. Aurousseau, …, R. Blunck. 2012. Automating single subunit counting of membrane proteins in mammalian cells. *J. Biol. Chem.* 287:35912–35921.
26. Bumb, A., S. K. Sarkar, …, K. C. Neuman. 2011. Quantitative characterization of fluorophores in multi-component nanoprobes by single-molecule fluorescence. *Biomed. Opt. Express.* 2:2761–2769.
27. Hines, K. E. 2013. Inferring subunit stoichiometry from single molecule photobleaching. *J. Gen. Physiol.* 141:737–746.
28. Arellano, R. O., and R. Miledi. 1995. Functional role of follicular cells in the generation of osmolarity-dependent Cl^- currents in *Xenopus* follicles. *J. Physiol.* 488:351–357.
29. Voets, T., G. Buyse, …, B. Nilius. 1996. The chloride current induced by expression of the protein pICln in *Xenopus* oocytes differs from the endogenous volume-sensitive chloride current. *J. Physiol.* 495:441–447.
30. Simonin, A., N. Montalbetti, …, M. A. Hediger. 2015. The hydroxyl side chain of a highly conserved serine residue is required for cation selectivity and substrate transport in the glial glutamate transporter GLT-1/SLC1A2. *J. Biol. Chem.* 290:30464–30474.
31. Yahara, T., M. Tachikawa, …, K. Hosoya. 2014. Amino acid residues involved in the substrate specificity of TauT/SLC6A6 for taurine and γ-aminobutyric acid. *Biol. Pharm. Bull.* 37:817–825.
32. Preston, G. M., T. P. Carroll, …, P. Agre. 1992. Appearance of water channels in *Xenopus* oocytes expressing red cell CHIP28 protein. *Science.* 256:385–387.
33. Fields, R. D., and Y. Ni. 2010. Nonsynaptic communication through ATP release from volume-activated anion channels in axons. *Sci. Signal.* 3:ra73.
34. Abascal, F., and R. Zardoya. 2012. LRRC8 proteins share a common ancestor with pannexins, and may form hexameric channels involved in cell-cell communication. *BioEssays.* 34:551–560.
35. Boassa, D., C. Ambrosi, …, G. Sosinsky. 2007. Pannexin1 channels contain a glycosylation site that targets the hexamer to the plasma membrane. *J. Biol. Chem.* 282:31733–31743.
36. Ambrosi, C., O. Gassmann, …, G. E. Sosinsky. 2010. Pannexin1 and Pannexin2 channels show quaternary similarities to connexons

and different oligomerization numbers from each other. *J. Biol. Chem.* 285:24420–24431.

37. Penuela, S., R. Gehi, and D. W. Laird. 2013. The biochemistry and function of pannexin channels. *Biochim. Biophys. Acta.* 1828:15–22.
38. Ulbrich, M. H., and E. Y. Isacoff. 2007. Subunit counting in membrane-bound proteins. *Nat. Methods.* 4:319–321.
39. Hyzinski-García, M. C., A. Rudkouskaya, and A. A. Mongin. 2014. LRRC8A protein is indispensable for swelling-activated and ATP-induced release of excitatory amino acids in rat astrocytes. *J. Physiol.* 592:4855–4862.
40. Hammer, C., P. Wanitchakool, …, K. Kunzelmann. 2015. A coding variant of ANO10, affecting volume regulation of macrophages, is associated with Borrelia seropositivity. *Mol. Med.* 21:26–37.
41. Blumenthal, E. M., and L. K. Kaczmarek. 1994. The minK potassium channel exists in functional and nonfunctional forms when expressed in the plasma membrane of *Xenopus* oocytes. *J. Neurosci.* 14:3097–3105.
42. Chillarón, J., M. Font-Llitjós, …, M. Palacín. 2010. Pathophysiology and treatment of cystinuria. *Nat. Rev. Nephrol.* 6:424–434.
43. Birkenhäger, R., N. Prera, …, S. Arndt. 2014. A novel homozygous mutation in the EC1/EC2 interaction domain of the gap junction complex connexon 26 leads to profound hearing impairment. *BioMed Res. Int.* 2014:307976.
44. Eertmoed, A. L., Y. F. Vallejo, and W. N. Green. 1998. Transient expression of heteromeric ion channels. *Methods Enzymol.* 293:564–585.
45. Minieri, L., H. Pivonkova, …, S. Ferroni. 2015. Intracellular Na^+ inhibits volume-regulated anion channel in rat cortical astrocytes. *J. Neurochem.* 132:286–300.
46. Mongin, A. A. 2016. Volume-regulated anion channel—a frenemy within the brain. *Pflugers Arch.* 468:421–441.
47. Voets, T., G. Droogmans, …, B. Nilius. 1999. Reduced intracellular ionic strength as the initial trigger for activation of endothelial volume-regulated anion channels. *Proc. Natl. Acad. Sci. USA.* 96:5298–5303.
48. Smits, G., and A. V. Kajava. 2004. LRRC8 extracellular domain is composed of 17 leucine-rich repeats. *Mol. Immunol.* 41:561–562.
49. Dourado, M., E. Wong, and D. H. Hackos. 2014. Pannexin-1 is blocked by its C-terminus through a delocalized non-specific interaction surface. *PLoS One.* 9:e99596.
50. Engelhardt, K., M. Schmidt, …, R. Dermietzel. 2015. Effects on channel properties and induction of cell death induced by C-terminal truncations of pannexin1 depend on domain length. *J. Membr. Biol.* 248:285–294.
51. Sandilos, J. K., and D. A. Bayliss. 2012. Physiological mechanisms for the modulation of pannexin 1 channel activity. *J. Physiol.* 590:6257–6266.
52. Sandilos, J. K., Y. H. Chiu, …, D. A. Bayliss. 2012. Pannexin 1, an ATP release channel, is activated by caspase cleavage of its pore-associated C-terminal autoinhibitory region. *J. Biol. Chem.* 287:11303–11311.
53. Stühmer, W. 1998. Electrophysiologic recordings from *Xenopus* oocytes. *Methods Enzymol.* 293:280–300.
54. Bröer, S. 2010. *Xenopus laevis* oocytes. *Methods Mol. Biol.* 637:295–310.
55. Gandhi, C. S., and R. Olcese. 2008. The voltage-clamp fluorometry technique. *Methods Mol. Biol.* 491:213–231.